THE JOURNAL OF PHYSICAL CHEMISTRY B

ARTICLE

pubs.acs.org/JPCB

Amphiphilic Behavior of New Cholesteryl Cyclodextrins: A Molecular Study

Martin Bauer,[†] Christophe Fajolles,[†] Thierry Charitat,[‡] Hanna Wacklin,[§,⊥] and Jean Daillant*[,†]

[†]CEA, IRAMIS, SIS2M, LIONS, UMR 3299 CEA/CNRS, CEA-Saclay bât. 125, F-91191 Gif-sur-Yvette Cedex, France

[‡]Université de Strasbourg, Institut Charles Sadron, CNRS, 23 Rue du Loess, BP 84047, 67034 Strasbourg Cedex 2, France

[§]Institut Laue-Langevin, 6 rue Jules Horowitz, BP 156, 38042 Grenoble Cedex, France

Supporting Information

ABSTRACT: Amphiphilic cyclodextrins (CDs) are good candidates to functionalize natural membranes as well as synthetic vesicles. In this paper, we describe the synthesis of the amphiphilic permethylated monocholesteryl α-CD (TASC). Its interfacial behavior is compared with that of the permethylated mono- and dicholesteryl β-CD analogues (TBSC and TBdSC). Langmuir isotherms suggest a reorganization upon compression for all compounds, which is quantified using neutron as well as X-ray reflectivity. The in-plane structure is characterized by atomic force microscopy (AFM) on monolayers deposited on solid substrates. A model involving a reorientation of the CD with respect to the interface to adjust its conformation to the available area per molecule is proposed. Although we observe for TBSC a rearrangement similar to TASC and TBdSC, it is already achieved at lower surface pressures compared with its disubstituted derivative. This specific behavior is explained by an increased structural flexibility and compressibility compared with TBdSC and TASC. The average number of water molecules per CD was determined using the neutron data and validated from X-ray data, which also allows the determination of the CD's molecular volume. The permethylated CD molecules are strongly hydrated in the film, but the α-CD analogue is less hydrated than the β-CD derivatives, and hydration decreases with compression.

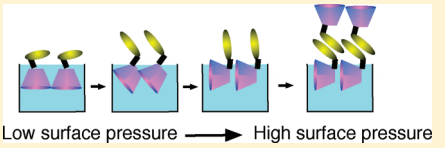

INTRODUCTION

Cyclodextrins (CDs) are natural cyclic oligosaccharides with a truncated cone shape and a hydrophobic cavity that enables them to form host−guest complexes with appropriate molecules. The most abundant α-, β- and γ-CDs are built of six, seven, and eight glucose units, respectively. Since CDs possess a large set of readily modified hydroxyl groups, these cyclic oligosaccharides have become valuable precursors for supramolecular chemistry.[1] The construction of amphiphilic CDs is of particular interest because it combines the CD's ability to act as host molecule with the amphiphiles' capability to self-assemble to supramolecular structures such as vesicles, bilayers, or nanoparticles.[2,3] Recent advances in CD synthetic modification methods allowed practical preparations of selectively disubstituted α- and β-CDs. This has attracted a new interest in amphiphilic CDs, so far restricted mainly to monosubstituted, statistically or persubstituted derivatives.[3]

Thus, 6I,6IV-(β-cholesteryl)succinylamido-6I,6IV-(6-deoxy-per-(2,3,6-*O*-methyl))cycloheptaose, abbreviated TBdSC (Figure 1), which is a disubstituted β-CD bearing two cholesterol residues,[4] was recently described. It can be readily obtained from permethylated 6A,6D-modified β-CD.[5] The succinate linker had been determined as an appropriate linker, long enough to ensure relative mobility of the CD and cholesteryl moieties, short enough to avoid self-inclusion, and allowing sufficient mobility (or degrees of freedom) to ensure conformational adaptability.[6]

A close-up study of TBdSC has revealed that it readily inserts into DPPC monolayers to form mixed monolayers for low pressure, whereas segregation occurs for high surface pressure. Moreover, high lateral pressure also induces a reorientation of the CD cavity axis, as demonstrated particularly for monolayers of pure TBdSC. Two selectively grafted cholesterols modify the hydrophilic/hydrophobic balance, but also create a rotation axis defined by the two substituted residues on the CD primary rim, allowing rotation and a consequent decrease of its surface area.[7]

These results prompted us to explore the specific influence of cholesterol and CD, which are the hydrophobic and hydrophilic moieties, respectively, on the amphiphilic behavior. Therefore, monocholesteryl analogues were prepared from permethylated β- and α-amino-CDs. These three molecules were at first studied and compared as pure Langmuir monolayers.

In this paper, we fully describe the air−water interface behavior of pure TBdSC and its monocholesteryl β- and α-CD analogues, called TBSC and TASC (Figure 1). Compression isotherms suggest the same type of reorganization upon compression. By reflectivity measurements, it is shown to consist of a reorientation of the CD moiety, whose axis rotates from perpendicular to parallel arrangement with respect to the water surface. However, the scenarios of these reorganizations are markedly

Received: June 23, 2011
Revised: October 28, 2011
Published: November 09, 2011

ACS Publications © 2011 American Chemical Society

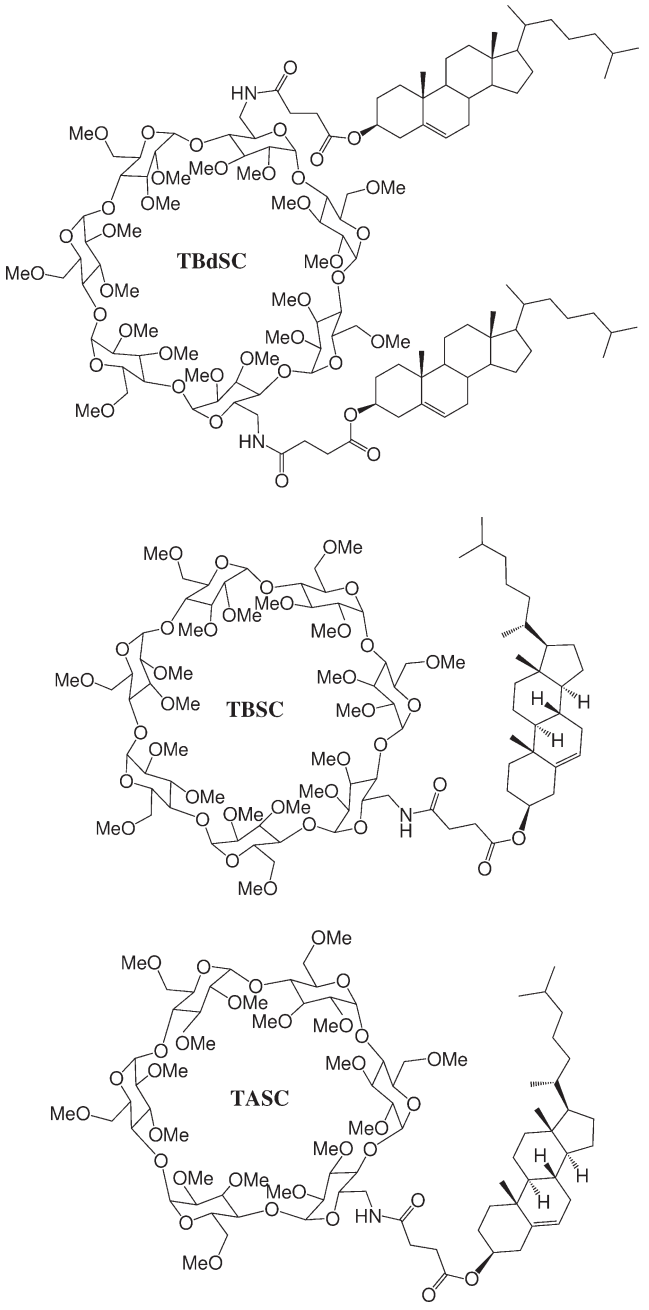

Figure 1. Chemical structure of TBdSC, TBSC, and TASC.

different and strongly depend on flexibility and compressibility, which are determined by the number of attached hydrophobic anchors and the size of the CD. This is evidenced by the isotherm and reflectivity data. It is then correlated to the in-plane structures, which are characterized using atomic force microscopy (AFM) on monolayers deposited on solid substrates.

EXPERIMENTAL SECTION

Synthesis. TBdSC and TBSC are reported in a previous paper.[7] TASC preparation differs noticeably. Indeed, the common DCC-based coupling method[4] used to create the amide was found to induce a partial, and still unexplained, oxidation at C-7 on the cholesteryl residue as a carbonyl function. Therefore, TASC **5** (Scheme 1) is alternatively synthesized in three steps, starting from 6^I-azido-6^I-deoxy-cyclomalto- hexaose (monoazido-α-CD) **1** (Scheme 1). The first steps are transposed from Jicsinszky's procedure.[8] A methylation step with methyl iodide and sodium hydride in DMF is followed by a reduction of the azido group to an amine with Pd/C as catalyst and hydrazine hydrate as hydrogen donor. The last step is slightly adapted from a method recently reported by Mukaiyama et al.[9] to use common reagents. The cholesteryl hemisuccinate **4** is in situ-activated with toluenesulfonic anhydride (Ts_2O) as a mixed anhydride in the presence of DMAP to yield the amide in a clean and efficient manner. Procedures and spectra can be found in the Supporting Informations.

Langmuir Monolayers. The surface pressure/area isotherms were measured with a temperature-controlled Langmuir balance (702BAM Film Balance for Brewster Angle Microscopy, Micro-Processor Interface IU4, NIMA Technology) used in conjunction with a Brewster angle microscope (BAM). It possesses a maximum surface area of 700 cm^2, a minimum surface area of 80 cm^2, and is filled with ~500 mL of ultrapure water (18.2 MΩ·cm) subphase. The trough, placed on an antivibration table, is covered by a plastic hood. The compounds are dissolved in chloroform (Riedel-de Haen, EtOH stab.), and the solution is spread with a Hamilton syringe. Typical spreading volumes are 50 μL. The surface pressure is measured by the Wilhelmy plate method using a filter paper. After 10 min of equilibration of the monolayer, the isotherms are recorded with a compression speed of 10 cm^2/min and at a temperature of 20 °C if not mentioned differently.

Atomic Force Microscopy. Langmuir−Blodgett (LB) films of the monolayers were deposited onto hydrophilic, freshly cleaved mica wafers for several surface pressures at the air−water interface with a dipper speed of 1 mm/min. Typically, transfer ratios >0.9 were obtained. The films were then examined in tapping mode with a Nanoscope V (Veeco) AFM. Standard cantilevers with a conical silicon etched probe tip (NSC15, μmasch) with typical spring constants on the order of 40 N/m, as determined by the thermal resonance method, and typical resonance frequencies on the order of 350 kHz were used. Images with scan sizes of 1 μm × 1 μm and 3 μm × 3 μm were recorded with scan rates of 1 and 0.5 Hz, respectively.

Neutron Reflectivity. The neutron reflectivity experiments were carried out at the time-of-flight reflectometer Figaro (Fluid Interfaces Grazing Angles Reflectometer) at the ILL, Grenoble.[10] The incoming beam comprises wavelengths between 2 and 30 Å. For our samples, a q range from 0.005 to 0.30 $Å^{-1}$ could be achieved by joining together two measurements with a reflection angle, $\Theta_1 = 0.62°$ and $\Theta_2 = 3.82°$ as well as a wavelength resolution of 5.6%. The samples were measured in a Langmuir trough (Nima) that is filled with a D_2O subphase. Its maximum and minimum area are 930 and 254 cm^2, respectively. The reflectivity was normalized by direct beams in a transmission geometry through the windows of the Langmuir trough lid and corrected for incoherent background scattering. The data were fitted with the Motofit package,[11] where the specular reflectivity is calculated by the Abeles matrix method for stratified interfaces.[12] A detailed description of the Motofit software is given elsewhere.[13]

X-ray Reflectivity. Complementary to neutron reflectivity, the thickness and vertical composition of the monolayers were also characterized by X-ray reflectivity. The monolayers were spread on a water subphase in a homemade Teflon trough with a

Scheme 1. Three-Step Synthesis of TASC 5

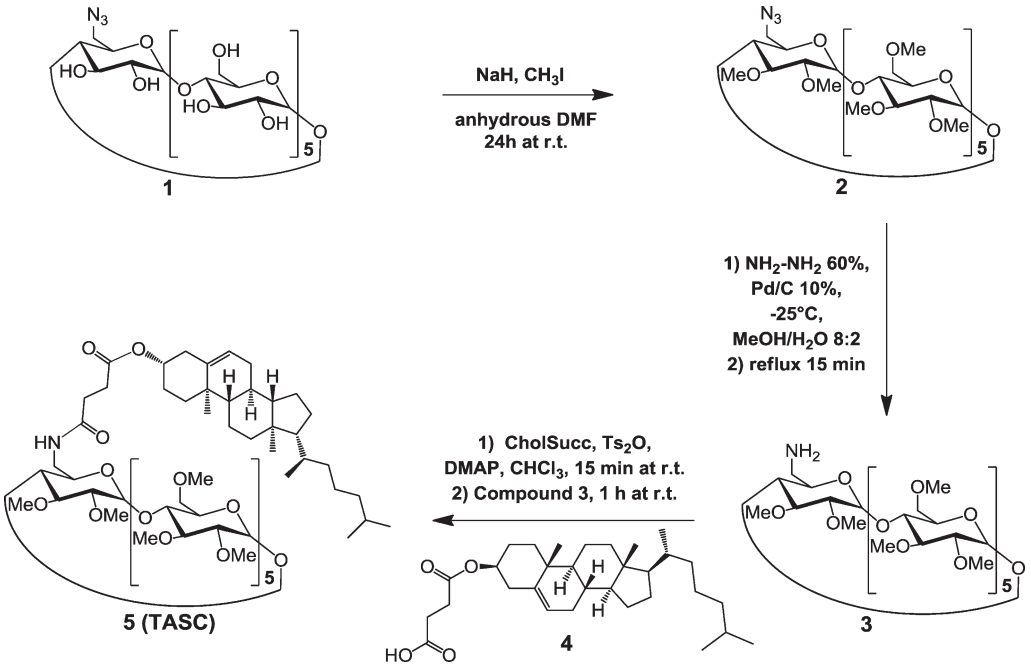

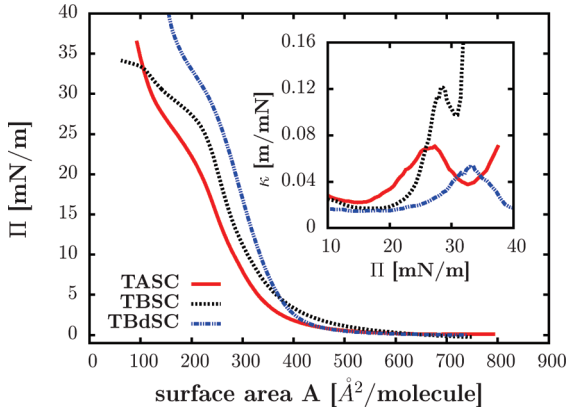

Figure 2. Langmuir isotherms and isothermal compressibility (inset) at 20 °C: (a) TASC, (b) TBSC, and (c) TBdSC.

maximum and minimum area of 462 and 161 cm^2, respectively, suitable to fit into a Siemens powder diffractometer D5000. A movable Teflon barrier allows compression of the monolayer to the desired surface pressure for the X-ray reflectivity measurement. The trough and the diffractometer were operated with homemade software. The Cu K_α beam (wavelength λ_x = 1.54 Å) is first collimated using 100 μm slits. A graphite monochromator is placed after the sample in front of the NaI scintillator detector. The homemade software allows one to record rocking curves at each point of the reflectivity curve. The data were also fitted with the Motofit software applying the same model as used for the neutron reflectivity.

RESULTS

Langmuir Isotherms. The surface-pressure area isotherms for (a) TASC, (b) TBSC, and (c) TBdSC are shown in Figure 2. For TASC and TBSC, no significant temperature dependence can be observed (as opposed to TBdSC[7]), and BAM images feature aggregates that increase in number with the surface pressure Π and decrease in molecular surface area A.

All the isotherms are reproducible for the same spreading conditions, and in addition, no hysteresis is observed for isotherm cycles. All three isotherms exhibit a sharp rise beginning at A = 350 Å^2 for TASC, A = 380 Å^2 for TBSC and A = 400 Å^2 for TBdSC. They also show a pseudoplateau at high surface pressures. The isothermal surface compressibility,

$$\kappa_S = -\frac{1}{A}\frac{dA}{d\Pi} \quad (1)$$

is plotted in the inset of Figure 2 to emphasize the pseudoplateau because it shows local maxima for first-order phase transitions. κ_S was calculated numerically from the data obtained from the Langmuir isotherms as

$$\kappa_S = -\frac{1}{A_i}\frac{(A_{i+1} - A_i)}{(\Pi_{i+1} - \Pi_i)} \quad (2)$$

To minimize the noise due to the differentiation of the discrete data, 10 data points have been averaged to give a smoother compressibility graph. The compressibility curves for the three CDs show pronounced peaks for the pseudoplateau at Π = 25 mN/m for TASC, Π = 27 mN/m for TBSC, and Π = 32 mN/m for TBdSC (Figure 2). For TBSC, the compressibility rises strongly after the pseudoplateau peak, which, together with the flat continuation of the isotherm, is an indication for a film collapse. The TASC and the TBdSC isotherms look very much alike, apart from the rise at different surface areas, yet the TBSC starts rising slowly for large surface areas and continues rather flat after the pseudoplateau.

Reflectivity Measurements. Neutron and X-ray reflectivity experiments have been carried out to determine the film thickness

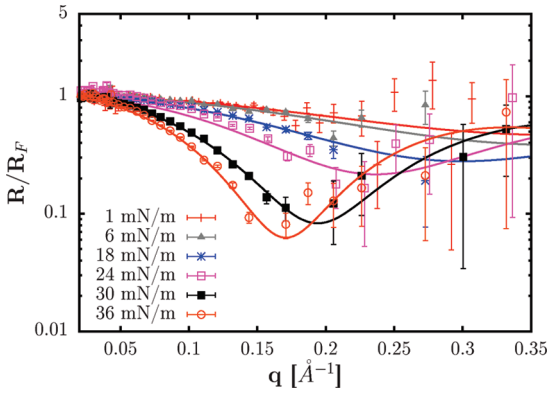

Figure 3. Neutron reflectivity curves at different surface pressures from top to bottom for TASC (red +, 1 mN/m; gray ▲, 6 mN/m; blue ★, 18 mN/m; red □, 24 mN/m; ■, 30 mN/m; red ○, 36 mN/m). Only a part of the recorded scattering curves is displayed in the graph so that they remain distinguishable.

and density profile to elucidate the nature of the pseudoplateau in the isotherms.

To obtain a better contrast and to avoid incoherent scattering, D_2O has been used as subphase for the neutron reflectivity instead of normal water, which is used for the X-ray scattering. The shapes of the isotherms are very similar for both subphases. Thus, the results for both methods can be directly compared. However, due to a limited compression range of the Langmuir trough available for the neutron experiment, more compound had to be spread on the surface to reach the desired surface pressures, leading to a slight shift to higher surface areas (10 - 20 Å^2) for the isotherms. Furthermore Langmuir isotherms are known to be shifted when using D_2O as subphase.[14] Therefore, the molecular areas from the isotherms recorded on the D_2O subphase are used for calculations with the data from the neutron experiments.

Looking at the reflectivity curves in Figure 3, it can be clearly seen that for all three modified CDs, a minimum appears with increasing surface pressure that is related to a structural change in the film. Starting at surface pressures around the pseudoplateau, the scattering curve minimum drastically deepens. This behavior is most pronounced for TBSC, for which we observe a very large step between the curves for surface pressures below and above the pseudoplateau.

Complementary X-ray scattering experiments have been measured only for TASC and TBdSC for two points in the isotherm, one below and one above the phase transition, and similar to the neutron experiment, the curves at low surface pressures are very different from the ones obtained at high pressures (the X-ray curves can be found in the Supporting Information). The data obtained from neutron and X-ray scattering are fitted with the same model. The measured curves are fitted using a two-layer box model (represented on top in Figure 4) with two distinct regions of scattering length densities (SLD_1, SLD_2) and electron density (ED_1, ED_2), respectively, as well as the corresponding thicknesses l_1, l_2. The top layer, 1, can be assigned to the hydrophobic cholesterol, and the bottom layer, 2, to the hydrophilic CD residues. For TBSC at Π = 32 mN/m, a third layer had to be added to the model to fit the data properly. The subphase roughness was 3 ± 1 Å for all fits, and the roughnesses for the CD and cholesteryl layers are in the range between 2 and 4 Å.

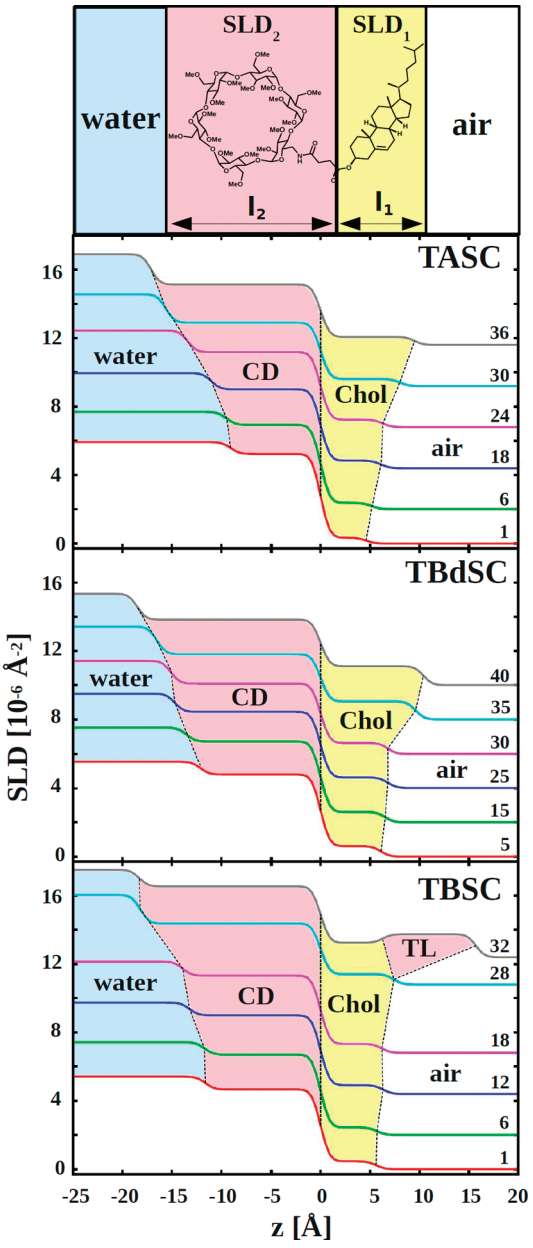

Figure 4. SLD profiles from neutron reflectivity experiments at different surface pressures for TASC, TBdSC, and TBSC. The surface pressures corresponding to each SLD profile are indicated on the right side of the graph in milli-Newtons per meter. To account for better legibility, the curves have been consecutively shifted proportionally to the surface pressure Π (2×10^{-6} Å^{-2} for 5 mN/m). TL signifies the additional layer that had to be added for TBSC at 32 mN/m.

Comparing the overall thickness of the films shows that, for low surface pressures, the TASC monolayer is ∼15 Å, and that for TBdSC and TBSC is ∼18 Å thick. For high surface pressures, the film thickness increases to ∼27 Å for TASC, to ∼29 Å for TBdSC, and to ∼33 Å for TBSC (all values obtained from the fits can be found in the corresponding tables in the Supporting Information). This behavior is clearly visualized in the scattering length density profiles displayed in Figure 4.

TASC. Having a closer look at the CD part of the monolayer reveals that for TASC, the CD film thickness stays in the range of 10−11 Å up to surface pressures close to the pseudoplateau

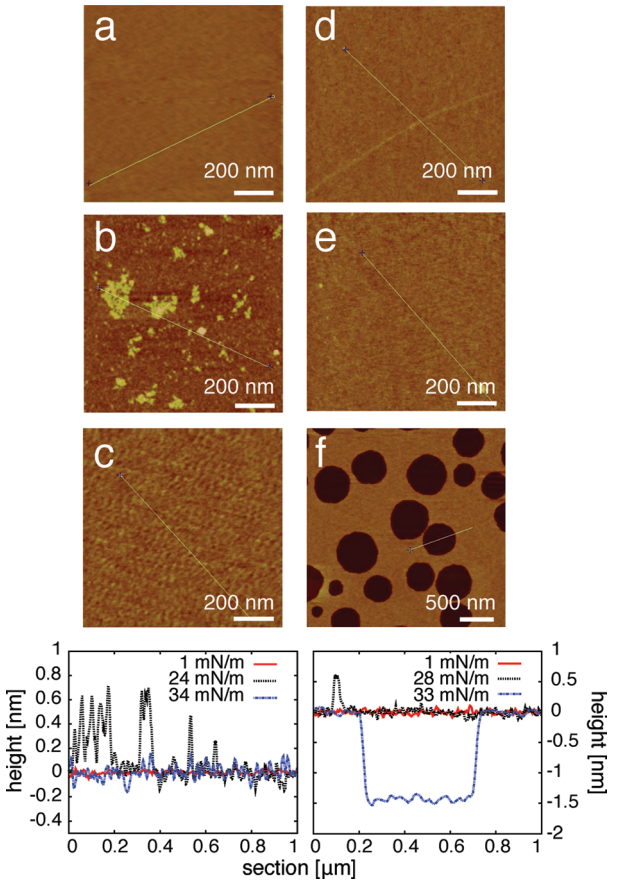

Figure 5. AFM images and profiles for TASC (left) and TBSC (right). Π = (a) 1, (b) 24, (c) 35, (d) 1, (e) 28, and (f) 33 mN/m.

(Figures 4 and 7). Starting from Π = 21 mN/m, the size of the CD layer increases steadily from 11 to 17 Å at 36 mN/m. The film compression is accompanied by a drop in scattering length density from 5.2 × 10^{-6} to 3.6 × 10^{-6} $Å^{-2}$. Likewise, the X-ray experiments reveal a jump in electron density from 0.39 to 0.43 $Å^{-3}$. X-ray and neutron reflectivity curves are fitted with the same model. As the X-ray data extend to higher q values, they better resolve the cholesteryl layer whose thickness was constrained to the X-ray values for the neutron fits. It increases from 4.5 to 10 Å with compression (see corresponding data in Supporting Information). The scattering length density is on the order of 0.4 × 10^{-6} $Å^{-2}$ for all surface pressures.

TBdSC. For TBdSC, the CD layer is ∼12.5 Å thick at the beginning of compression (Figure 4). Starting from surface pressures close to the pseudoplateau, its size increases significantly to ∼18.5 Å. Furthermore the scattering length density decreases from 4.8 × 10^{-6} to 3.8 × 10^{-6} $Å^{-2}$, as well as the electron density increases from 0.38 to 0.44 $Å^{-3}$.

The cholesteryl layer increases from 6 to 10 Å for Π = 40 mN/m. The X-ray data gives comparable results, with a rise from 6 to 11.5 Å (see the Supporting Information).

TBSC. The CD layer of TBSC exhibits a thickness between 11.5 Å for low surface pressures and 14 Å at Π = 18 mN/m. Then the size increases drastically to 18 Å at 28 mN/m (Figure 4), like for TASC and TBdSC coming along with a drop in scattering length density from 4.7 × 10^{-6} to 3.6 × 10^{-6} $Å^{-2}$. The cholesteryl layer increases from 5.5 to 7.5 Å at Π = 28 mN/m.

For Π = 32 mN/m, a three-layer model had to be applied to fit the curve. Good fits could only be obtained by adding the layer on top of the cholesteryl layer, whereas fitting the data, adding the third layer on the CD side (subphase) was not successful. We find that the CD layer remains ∼18 Å thick. The scattering length density is increased to 4.1 × 10^{-6} $Å^{-2}$, which is higher than for Π = 28 mN/m. For the middle layer, a thickness of 6.3 Å and scattering length density of 0.8 × 10^{-6} $Å^{-2}$ is found. The additional top layer has a size of 9.5 Å with a scattering length density of 1.3 × 10^{-6} $Å^{-2}$. Moreover, the top-layer roughness (6 Å) is larger than that of the other layers (2−3 Å).

AFM. To investigate the in-plane structure of the monolayer, several Langmuir−Blodgett films on mica have been prepared for different surface pressures and imaged by AFM.

For TASC, the monolayer is very flat and homogeneous at low pressure (Figure 5a). An image at the pseudoplateau (Figure 5b) shows ∼7 Å high domains as well as an increased roughness (∼3 Å). At 34 mN/m (Figure 5c), the surface is again homogeneous, whereas the profile indicates that the roughness is larger compared with the low pressure image.

For low surface pressure, the Langmuir−Blodgett film of TBSC (Figure 5d) is very flat and homogeneous, similar to TASC. At 28 mN/m (Figure 5e), there are no domains visible, and only a small increase in roughness can be observed. Figure 5f, which is taken on the flat part of the isotherm at 33 mN/m, shows characteristic holes of ∼15 Å depth and diameters of several hundreds of nanometers. It exhibits a roughness similar to that of the image in Figure 5e.

DISCUSSION

Amphiphilic Behavior. All three investigated amphiphilic CDs show truly amphiphilic behavior and form stable monolayers, since isotherms can be recorded up to very high surface pressures before film collapse occurs. The sharp increase in the TASC isotherm occurs for smaller surface areas ($A \approx 350$ $Å^2$) compared with TBSC ($A \approx 380$ $Å^2$) and TBdSC ($A \approx 400$ $Å^2$), which reflects the smaller size of the α-CD moiety in the former molecule. This observation, as well as the CDs' much larger volume compared with the cholesterol residue leads us to the conclusion that the shape of the isotherms is determined mainly by the CD part of the molecules. According to the literature, the β-CD exhibits a higher structural flexibility compared with the α-CD.[15,16] Indeed, in addition to the degrees of freedom due to the unique succinic linker, it is possible for a glucopyranose unit, typically the one grafted by the hydrophobic moiety, to spin about its glycosidic bond.[17] This should be much easier for β-CD than for the more sterically constrained α-CD. This higher deformability is the reason for the different isotherm shapes for TASC and TBSC (Figure 2). In TBdSC, the rigidity of the usually rather flexible β-CD moiety is restricted by the two cholesteryl residues, explaining an isotherm shape similar to TASC, as well as a similar compressibility at the pseudoplateau (Figure 2). The slow rise for a very large surface area ($A \approx 600$ $Å^2$) and the sharp increase for smaller surface areas compared with TBdSC also reflect the greater flexibility of the TBSC.

Monolayer Morphology. *CD Layer.* Every isotherm of the investigated CDs shows a pseudoplateau that corresponds to a structural change in the monolayer. Looking at the CD part of the monolayer in more detail reveals for all investigated amphiphiles that the thickness increases significantly, about 6−7 Å, when comparing surface pressures below and above the pseudoplateau.

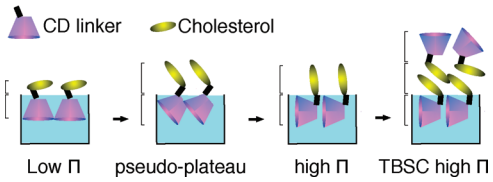

Figure 6. Change of conformation in the CD layer.

The compression of the film is accompanied by a drop in scattering length density in the neutron reflectivity experiment, which corresponds to an expulsion of water from the film, which is further discussed in the following section.

According to the literature, the torus height for methylated α- and β-CD is increased from 8 to 11 Å compared with the native compounds due to the methyl groups.[18] Our data for low pressure correspond well to these values. However, we find that for TASC, the CD layer is ~2 Å thinner compared with TBdSC and TBSC. This suggests that the smaller α-CD headgroup has a small influence on the torus height.

The X-ray and neutron results give a clear interpretation of the pseudoplateau in the isotherms. The CD layer thickness is, indeed, equal to the methylated CD height for low surface pressures and to its diameter[1,19] at large surface pressures. The transformation occurring at the pseudoplateau is a conformational change, where the axis of the CD's cavity rotates from perpendicular to parallel to the surface (Figure 6). For nonmethylated native amphiphilic CDs, such a reorientation has already been confirmed by IRRAS measurements at the air−water interface.[20] The rearrangement occurs gradually, ~1.5 Å every 3 mN/m, starting from the pseudoplateau with the CD's axis being aligned more and more parallel with respect to the surface (Figure 6). Furthermore, the AFM images for TASC at the pseudoplateau (Figure 5b) exhibit domains with the same distinct height of 6 Å, corresponding to the difference between CD height and diameter, indicating a coexistence between the two conformations. AFM images at high pressure show again a homogeneous, flat surface, with the whole monolayer aligned in its high-pressure conformation.

For TBSC, the neutron reflectivity data suggest that the conformational change already occurs for lower surface pressures than for the disubstituted TBdSC. With further compression for surface pressures above 30 mN/m, the flat continuation of the isotherm reveals the beginning of the film collapse. This is also reflected in the neutron data at 32 mN/m, where an additional third layer on top of the cholesteryl layers is now required to successfully fit the reflectivity data. Since addition of a third layer close to the subphase does not give good fits, film buckling toward the solution is not a likely explanation. The third layer most probably consists of a TBSC double layer with a very disordered top layer, indicated by its high roughness (6 Å) compared with the other slabs (3 Å) and all other fits, where the roughness is on the order of 2−3 Å. Because the transfer ratios are always larger than 90%, the holes in the AFM image at Π = 34 mN/m (Figure 5f) cannot be due to a loss of material during the transfer. They are consistent with a partial bilayer formation where zones of monolayer remain; they also explain a drastically decreased SLD of the top layer as an average between the holes and the elevated regions is measured.[21] The low scattering length density of the top layer also indicates that the CDs are only very little hydrated compared with the CDs situated in the layer close to the water.

Cholesteryl Layer. The thickness of the cholesteryl layer is determined mainly by the available surface area due to the CD moiety. It increases with compression from 4.5 to 10 Å for the monosubstituted α-CD and from 5 to 7.5 Å for the β-CD derivative because the bulkier β-CD leaves more space for the cholesteryl moiety. Similarly, the two cholesteryl moieties of TBdSC require more space, leading to a more pronounced increase in cholesteryl layer thickness with compression (6−11 Å). The more compact packing of the TBdSC's cholesteryl layer is also reflected in the significantly increased scattering length and electron densities for high pressures, in contrast to the monosubstituted molecules. Values reported in the literature for a fully stretched cholesterol molecule are ~17 Å.[22] At least part of the succinyl linker (~3 Å) should be assigned to the cholesteryl layer, explaining the elevated average SLD for the "cholesterol" slab compared with the expected cholesterol SLD (0.2×10^{-6} Å^{-2}),[23] since the SLD for the succinylic linker can be estimated to be on the order of 2.6×10^{-6} Å^{-2}. The effect seems to be most pronounced for TBdSC in high pressure conformation where the SLD for cholesterol is very much increased.

The tilt angles, Θ, for the cholesteryl part of the monolayer at maximum compression have been calculated from the expression

$$\cos \Theta = \frac{l_{\mathrm{Chol}}}{l_{\mathrm{st}}} \tag{3}$$

with the measured thickness of the cholesteryl layer, l_{Chol}, and the length of the fully stretched cholesteryl molecules, l_{st}, obtained from the literature.[22] The tilt angles decrease in the order TBSC (64°), TASC (55°), and TBdSC (50°), reflecting the available space of the cholesteryl residue in each compound. For low surface pressures, the cholesterol moieties are arranged almost flat on the surface. With rising compression, the increasingly smaller available surface area forces the cholesterol residues to arrange themselves more upright. However, for higher pressure, because the bulky CD residues determine the required surface area of the molecule, sufficient space remains for the cholesterol moieties to be tilted. In addition, for TBdSC, we observe an increase in the proportion of the linker group in the top layer.

Hydration of CD Headgroup. Methylated CDs are strongly hydrated in an aqueous environment.[24−26] Therefore, the CD layer in the film has a large water content. The number of water molecules per CD, n_{W}, can be calculated using the scattering length, $\mathrm{SLD_{CD}}$ (eq 4), and electron density, $\mathrm{ED_{CD}}$ (eq 5), extracted from the fits starting from the following definitions:

$$\mathrm{SLD_{CD}} = \frac{\mathrm{SL_{CD}} + n_{\mathrm{W}}\mathrm{SL_w}}{l_{\mathrm{CD}}A} \tag{4}$$

$$\mathrm{ED_{CD}} = \frac{N_{\mathrm{CD}} + n_{\mathrm{W}}N_{\mathrm{w}}}{l_{\mathrm{CD}}A} \tag{5}$$

where $\mathrm{SL_{CD}}$ (respectively, $\mathrm{SL_w}$) is the scattering length of the CD (respectively, D_2O), A is the surface area extracted from the isotherm, and l_{CD} is the corresponding length of the CD layer. N_{CD} is the number of electrons in the CD residue of the molecule, and N_{w} is the number of electrons in heavy water. For the neutron data, this leads to the expression (eq 6).

$$n_{\mathrm{W}} = \frac{\mathrm{SLD_{CD}}l_{\mathrm{CS}}A - \mathrm{SL_{CS}}}{V_{\mathrm{w}}\mathrm{SLD_w}} \tag{6}$$

The scattering length of water is substituted by $V_{\mathrm{w}} \times \mathrm{SLD_w}$, where V_{w} is the molecular volume of D_2O (30 Å^3) and $\mathrm{SLD_w}$ is

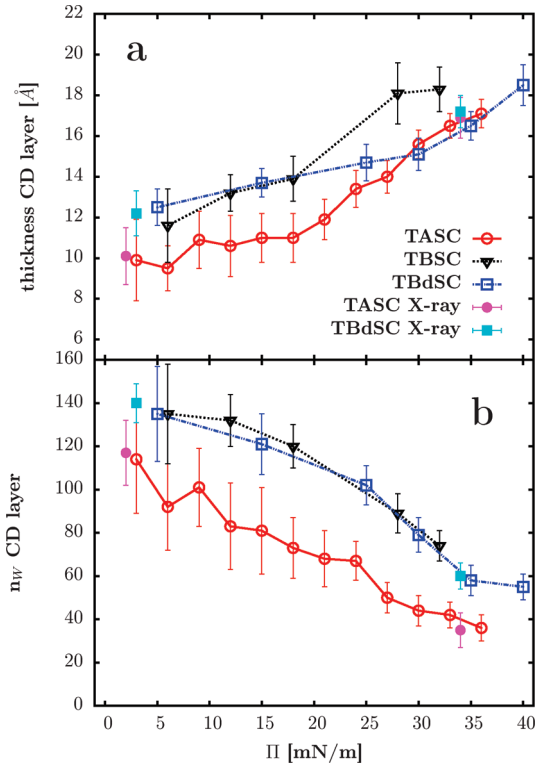

Figure 7. (a) CD layer thickness and (b) number of water molecules per CD for TASC (neutron, red ○; X-ray, red ●), TBSC (neutron, ▼) and TBdSC (neutron, blue □; X-ray, blue ■) during compression.

the scattering length density of the subphase, obtained from fitting the reflectivity curves. This is necessary because the values found for SLD_w (see the Supporting Information) are significantly lower than the literature value for pure heavy water (6.36×10^{-6} Å^{-2}).

Reference 27 shows that when the environment of the Langmuir trough is well controlled, there is no noticeable evolution of the bulk SLD. For the experiments described in this paper, using a sealed trough was not possible, and the bulk phase gets more enriched with normal water diffusing from the atmosphere at the D_2O−air interface. This is reflected in a decrease of SLD_w during the experiment (see the Supporting Information). For the X-ray experiments, n_W is expressed by

$$n_W = \frac{N_{CD} l_{CD} A - N_{CD}}{N_w} \tag{7}$$

Figure 7 shows the calculated number of water molecules per CD in the film for the different surface pressures. The values calculated from the X-ray data correspond very well to the results from the neutron scattering experiments. The water content decreases with rising compression for TASC from 114 to 36; for TBdSC, from 135 to 55; and for TBSC, from 193 to 74. The TASC molecule is the least hydrated because it possesses one glucose unit less than the two β-CD derivatives TBdSC and TBSC. The hydration behavior of TBSC and TBdSC is similar (Figure 7b), as expected because they possess chemically identical headgroups. The number of water molecules per CD we calculated for low surface pressures corresponds well to values reported for methylated CDs in the bulk phase.[25] At high surface pressures, we find that the CDs are less hydrated than in the bulk.[28] Looking at Figure 7b, the loss of water in the layer occurs slowly for low compression and then more rapidly from the pseudoplateau in the isotherm.

Table 1. Mean SLD_{CD-w} and ED_{CD-w} and Corresponding V_m for TASC, TBSC, and TBdSC

compound	SLD_{CD-w} (10^{-6}/Å^2)	V_{CD} (Å^3)	ED_{CD-w} (Å^{-3})	V_{CD} (Å^3)
TASC	2.15 ± 0.25	990 ± 280	0.540 ± 0.05	1300 ± 250
TBdSC	2.00 ± 0.20	1310 ± 220	0.550 ± 0.05	1530 ± 200
TBSC	1.80 ± 0.25	1320 ± 330		

Knowing n_W, it is possible to calculate x_W, the volume percentage of solvent content in the CD layer.

$$x_W = \frac{n_W V_w}{l_{CD} A} \tag{8}$$

By fixing the solvent penetration of the CD layer, the actual scattering length density, SLD_{CD-w}, and electron density, ED_{CD-w}, of the CD residues without water can be directly obtained from the fit. Thus, we have a means to estimate the molecular volume V_{CD} using (eq 9) for the neutron and (eq 10) for the X-ray data:

$$V_{CD} = \frac{sl_{CD}}{SLD_{CD\text{-}w}} \tag{9}$$

$$V_{CD} = \frac{N_{CD}}{ED_{CD\text{-}w}} \tag{10}$$

The calculated mean values of the scattering length density SLD_{CD-w}, as well as electron density ED_{CD-w} without water for the CD part and the corresponding molecular volumes V_m, are displayed in Table 1.

The SLD_{CD-w} as well as the ED_{CD-w} values are consistent with the ones found for bulk solutions of CDs (β-CD, $V = 1200$ Å^3; dimethyl-β-CD, $V = 1575$ Å^3) by Kuzmin et al.[28] As expected, the V_m for the methylated α-CD in TASC is smaller than for the β-CD derivatives. The V_m values from the neutron data are slightly smaller but within the error bars comparable to what has been reported for bulk solutions.[28] The decreased values could be due to the fact that we calculated the molecular volume as an average, since we assumed the V_m to stay constant during compression.

CONCLUSION

We demonstrated that the monosubstituted permethylated α-CD and β-CD derivative TASC and TBSC, like their disubstituted permethylated-β-CD analogue TBdSC, form stable monolayers because we are able to record Langmuir isotherms. The shape of the TASC isotherm resembles the one for TBdSC, with the only difference being that the pseudoplateau is shifted to lower surface pressures. Because of its small α-CD residue, the isotherm is also displaced to smaller surface areas for TASC. Interestingly, the TBSC behaves differently: its isotherm starts rising for large surface areas, and the monolayer collapses shortly after the pseudoplateau. To identify the structural change indicated by the pseudoplateau in the isotherms, we investigated the film morphology by reflectivity measurements and AFM. We found that, for all compounds, the CD residue undergoes a change in conformation during compression. At the phase transition, the CD residue rearranges from the cavity's axis aligned perpendicular with respect to the surface to an alignment parallel

to the surface (Figure 6). Although we observe for TBSC that a rearrangement of the CD layer occurs as for TASC and TBdSC, it is already achieved at lower surface pressures compared with its disubstituted derivative. The specific behavior of the TBSC is explained by the increased structural flexibility and compressibility compared with TBdSC and TASC. Furthermore the evolution of the hydration shell of the hydrophilic permethylated CD groups during compression has been assessed. The permethylated CD molecules are strongly hydrated in the film, and an average number of water molecules per CD could be determined. Considering the hydration of TASC, TBSC, and TBdSC, it is decreased for the α-CD analogue compared with its β-CD derivatives, and it decreases with compression. Knowing the number of water molecules in the film made it possible to calculate the average molecular volume for the CDs and confirm the values found in the literature.

Subsequent studies are underway to determine the insertion modes and solubility parameters of the compounds described here into phospholipid membranes. The knowledge and control of the conformational behavior of the hydrophilic CD head should be of importance to make the best use of amphiphilic CDs as versatile tools on natural or synthetic membranes as well as vesicles.

■ ASSOCIATED CONTENT

Supporting Information. Detailed synthesis of TASC as well as corresponding ^{1}H NMR, ^{13} NMR, ROESY, and MALDI-TOF spectra and HPLC chromatogram for TASC derivatives and complementary materials for X-ray and neutron reflectometry. This material is available free of charge via the Internet at http://pubs.acs.org/.

■ AUTHOR INFORMATION

Corresponding Author

*E-mail: Jean.Daillant@cea.fr.

Present Addresses

$^{\perp}$European Spallation Source ESS AB, P.O Box 176, SE-221 00 Lund, Sweden.

■ ACKNOWLEDGMENT

This work is supported by the French Research Program ANR-07-NANO-016-02 and Region Alsace (Ph.D. Grant). The authors thank Carlos Marques from the ICS Strasbourg for the coordination of the ANR project and his kind support. The authors also thank Maria Chiriac, Angelika Klaus, Mayeul Collot, and Jean-Maurice Mallet for their intervention in compound synthesis and Alain Valleix for advice in HPLC. In addition, we are grateful for the help and support of Giovanna Fragneto and Richard Campbell during the neutron experiment Figaro at the ILL, Grenoble.

■ REFERENCES

(1) Szejtli, J. *Chem. Rev.* **1998**, *98*, 1743–1753.
(2) Roux, M.; Perly, B.; Djedaini-Pilard, F. *Eur. Biophys. J.* **2007**, *36*, 861–867.
(3) Sallas, F.; Darcy, R. *Eur. J. Org. Chem.* **2008**, *6*, 957–969.
(4) Collot, M.; Garcia-Moreno, M.; Fajolles, C.; Roux, M.; Mauclaire, L.; Malleta, J. M. *Tetrahedron Lett.* **2007**, *48*, 8566–8569.
(5) Lecourt, T.; Mallet, J.; Sinay, P. *Carbohydr. Res.* **2003**, *338*, 2417–2419.
(6) Auzely-Velty, R.; Perly, B.; Taché, O.; Zemb, T. *Carbohydr. Res.* **1999**, *318*, 82–90.
(7) Klaus, A.; Fajolles, C.; Bauer, M.; Collot, M.; Mallet, J.-M.; Daillant, J. *Langmuir* **2011**, *27*, 7580–7586.
(8) Jicsinszky, L.; Ivanyi, R. *Carbohydr. Polym.* **2001**, *45*, 139–145.
(9) Funasaka, S.; Koji Kato, K.; Mukaiyama, T. *Chem. Lett.* **2007**, *36*, 1456–1457.
(10) FIGARO, Reflectometer at the ILL,http://www.ill.eu/instruments-support/instruments-groups/instruments/figaro/.
(11) Nelson, A. Co-refinement of multiple contrast neutron / X-ray reflectivity data using MOTOFIT. *J. Appl. Crystallogr.* **2006**, *39*, 273–276.
(12) Heavens, O. S. *Optical Properties of Thin Solid Films*; Dover Publications Inc.: Mineola, NY, 1992.
(13) Nelson, A. *J. Appl. Crystallogr.* **2006**, *39*, 273–276.
(14) Vaknin, D.; Kjaer, K.; Als-Nielsen, J.; Lösche, M. *Biophys. J.* **1991**, *59*, 1325–1332.
(15) Caira, M.; Bourne, S.; Mhlongo, W.; Dean, P. *Chem. Commun.* **2004**, *19*, 2216–2217.
(16) Steiner, T.; Saenger, W. *Carbohydr. Res.* **1996**, *282*, 53–63.
(17) Nishiyabu, R.; Kano, K. *Eur. J. Org. Chem.* **2004**, *2004*, 4988–4985.
(18) Immel, S.; Lichtenthaler, F. W. *Starch/Staerke* **1996**, *48*, 225–232.
(19) Dodziuk, H. In *Cyclodextrins and Their Complexes*; Dodziuk, H., Ed.; Wiley-VCH Verlag: Weinheim, 2006; pp 1−30.
(20) Vico, R.; de Rossi, R.; Maggio, B. *Langmuir* **2010**, *11*, 8407–8413.
(21) Coulon, G.; Daillant, J.; Collin, B.; Benattar, J.; Gallot, Y. *Macromolecules* **1993**, *26*, 1582–1589.
(22) Rapaport, H.; Kuzmenko, I.; Lafont, K.; Kjaer, S.; Howes, P.; Als-Nielsen, J.; Lahav, M.; Leiserowitz, L. *Biophys. J.* **2001**, *81*, 2729–2736.
(23) Demé, B.; Lee, L.-T. *J. Phys. Chem. B* **1997**, *101*, 8250–8258.
(24) Sultanem, C.; Moutard, S.; Benattar, J.; Diedaini-Pilard, F.; Perly, B. *Langmuir* **2004**, *20*, 3311–3318.
(25) Shikata, T.; Takahashi, R.; Satokawa, Y. *J. Phys. Chem. B* **2007**, *111*, 12239–12247.
(26) Jana, M.; Bandyopadhyay, S. *Langmuir* **2009**, *25*, 13084–13091.
(27) Romet-Lemonne, G.; Daillant, J.; Guenoun, P.; Yang, J.; Mays, J. *Phys. Rev. Lett.* **2004**, *93*, 148301.
(28) Kusmin, A.; Lechner, R.; Kammel, M.; Saenger, W. *J. Phys. Chem. B* **2008**, *112*, 12888–12898.